N9 Neuraminidase Complexes with Antibodies NC41 and NC10: Empirical Free Energy Calculations Capture Specificity Trends Observed with Mutant Binding Data†

William R. Tulip,‡,§ Vincent R. Harley,‡,∥ Robert G. Webster,⊥ and Jiri Novotny*,#

CSIRO Division of Biomolecular Engineering, 343 Royal Parade, Parkville, Victoria 3052, Australia, St. Jude Children's Research Hospital, Memphis, Tennessee 38101, and Department of Macromolecular Modeling, Bristol-Myers Squibb Research Institute, Princeton, New Jersey 08543-4000

Received September 22, 1993; Revised Manuscript Received March 3, 1994®

ABSTRACT: X-ray crystallographic coordinates of influenza virus N9 neuraminidase complexed with monoclonal antibodies NC41 and NC10 [Tulip et al. (1992) *J. Mol. Biol. 227*, 122–148] served as a starting point for calculations aimed at estimating free energy changes (ΔG) of complex formation between the two antibodies and the neuraminidase. Using an empirical function incorporating hydrophobic, electrostatic, and conformational entropy effects, we estimated contributions individual neuraminidase residues make to complex formation ($\Delta G_{residue}$) and compared the calculated values to experimentally measured differences in antibody binding between the wild-type and mutated neuraminidases [Nuss et al. (1993) *Proteins 15*, 121–132; calculations done without prior knowledge of the experimental data]. A good correspondence was found between the calculated $\Delta G_{residue}$ values and the mutant binding data in that side chains with large calculated ΔG contributions ($\Delta G_{residue} < -1$ kcal/mol) lie at sites of mutation which cause a marked reduction in antibody binding, and side chains for which $\Delta G_{residue} > -1$ kcal/mol are sites at which a mutation does not have a marked effect on binding. Because most of the $\Delta G_{residue} < -1$ kcal/mol side chains also make hydrogen bonds/salt bridges with the antibody, the correspondence of the effect of antibody binding with these electrostatic interactions (18 out of 27 for NC41 and, tentatively, 5 out of 7 for NC10) is about as good as that with predicted energetic residues. All the $\Delta G_{residue} < -1$ kcal/mol neuraminidase side chains cluster around the most protruding surface regions and are thus spread over different epitope segments. Surprisingly, different residues were found to make the most critical contributions to the NC41 and NC10 complex stabilities despite the fact that the NC41 and NC10 antigenic epitopes overlap, having ~70% of surface residues in common. It is thus possible, for two different antibodies, to recognize the same protein surface in strikingly different ways. As only a fraction of the neuraminidase residues appear to make large contributions to antibody binding, the results also support the hypothesis of a "functional" epitope in antigen–antibody interactions. Positive trends between both backbone rigidity and residue accessibility in the complexed state, and contributions of these residues to binding, were also observed for the NC41 complex.

The data base of crystal structures of antibody complexes now encompasses a broad range of haptens and macromolecular antigens (Davies et al., 1990). The interfaces in three lysozyme–Fab complexes (Amit et al., 1986; Bhat et al., 1990; Fischmann et al., 1991; Sheriff et al., 1987; Padlan et al., 1989), two neuraminidase–Fab complexes (Colman et al., 1987, 1989; Tulip et al., 1992a), and an Fab–antiidiotope Fab complex (Bentley et al., 1990) involve 13–19 contact residues and 690–916 Å^2 of buried molecular surface area on each molecule. The complementarity in shape is such that water molecules are excluded from most of the interacting surface. Chemical complementarity is mediated by 9–15 hydrogen bonds and up to 3 salt bridges between the protein antigen and antibody. Conformational changes are consistent with other protein–protein interactions (Colman, 1988; Janin & Chothia, 1990). Small changes (<2 Å) have been observed in the lysozyme antigen (Sheriff et al., 1987; Padlan et al., 1989) and the quaternary structure of the antibody (Bhat et al., 1990; Herron et al., 1991), with somewhat larger rearrangements of peptide antigens and of the CDR H3 loops (Stanfield et al., 1990; Rini et al., 1992).

These studies were highly illuminating but left many questions unanswered. How critical is the complementarity of shape and charge? Which contact residues and how many are favorable to binding, and which, if any, are repulsive? Do certain types of interactions or residue–residue pairings dominate energetically (Breyer & Sauer, 1989; Novotny et al., 1989; Jin et al., 1992; Nuss et al., 1993), or instead do most of the residues contribute comparably? Such questions involve simplifications of biophysical issues which, in their very nature, are quite complex. However, now that antibodies are being engineered for therapy (Reichmann et al., 1988), catalysis (Lerner et al., 1991), and various other functions (Winter & Milstein, 1991), a better understanding of the essential requirements of binding may be useful.

† W.R.T. received an Australian Postgraduate Research Award and a CSIRO Institute of Industrial Technologies Postgraduate Studentship. V.R.H. received a Commonwealth Postgraduate Research Award. R.G.W. was supported in part by U.S. Public Health Service Research Grant AI-29680 from the National Institute of Allergy and Infectious Disease, by Cancer Center Support (CORE) Grant CA-27165, and by the American Lebanese Syrian Associated Charities.

* To whom correspondence should be addressed.
‡ Division of Biomolecular Engineering.
§ Present address: G.P.O. Box 1336, Sydney, NSW 2001, Australia.
∥ Present address: Department of Genetics, University of Cambridge, Cambridge CB2 3EH, U.K.
⊥ St. Jude Children's Research Hospital.
Bristol-Myers Squibb Research Institute.

® Abstract published in *Advance ACS Abstracts,* June 1, 1994.

0006-2960/94/0433-7986$04.50/0

Table 1: N9 Neuraminidase Mutants: Comparison of NC41 Binding Data with Structural Data and Calculated $\Delta G_{residue}$ Values

	effect	complexed wild-type NA residue				uncomplexed wild-type NA residue	
mutant	binds NC41[a]	$\Delta G < -1$ kcal	H-bond to NC41[b]	SA[c] (Å^2)	$\langle B_{mc}\rangle$[d] (Å^2)	SA (Å^2)	$\langle B_{mc}\rangle$[d] (Å^2)
P328K	yes	no	no	14	15.5	38	17.7
N329D	yes	no	no	14	20.4	81	18.7
N329K	yes						
N344I	yes	no	yes	1	32.4	36	29.5
N345G	yes	no	no	53	30.9	94	30.3
S367N	no	yes	yes	0	8.7	18	12.3
S367G	no						
S367R	no						
S367T	no						
I368R	yes (I)	yes	yes	5	6.0	65	13.4
I368Y	yes (I)						
A369D	no	yes	yes	0	4.7	7.3	13.0
A369G	yes (II)						
S370L	no (III)	no	yes	6	5.9	25	15.7
S370A	yes						
S372Y	no (III)	no	yes	0	5.1	10	10.8
S372G	yes						
S372T	yes						
S372F	no (III)						
N400K	no	yes	yes	0	5.2	64	12.8
N400Q	no						
T401L	yes (IV)	yes	yes	4	6.7	138	15.4
W403G	yes	no	no	9	5.8	52	13.6
K432N	no	yes	yes	21	7.5	128	19.2
K432R	yes (V)						
K432D	no						
K432E/K435G[e]	no	yes	yes	105	14.6	129	23.2

[a] Binding data from Nuss et al. (1993) and Webster et al. (1987). "No" denotes that the mutant has markedly reduced binding in comparison with wild type. Trends are explained in the text, as are exceptions (I–V). [b] Hydrogen bonds are assigned using the criteria of Baker and Hubbard (1984) before energy minimization [for a list, see Table 7 in Tulip et al. (1992a)]. [c] Solvent-accessible surface area (Lee & Richards, 1971) is calculated with a 1.4-Å probe after energy minimization. [d] $\langle B_{mc}\rangle$, average main-chain temperature factor. [e] While data pertain to Lys 435, "yes" in column 3 refers to the additive ΔG values of Lys 432 and Lys 435.

Table 2: N9 Neuraminidase Mutants: Comparison of NC10 Binding Data with Structural Data and Calculated $\Delta G_{residue}$ Values[a]

	effect	complexed wild-type NA residue		
mutant	binds NC10	$\Delta G < -1$ kcal	H-bond to NC10	SA (Å^2)
N329D	no	yes	yes	0
S367N	yes	no	no	3
I368R	yes	no	no	0
A369D	no	yes	no	14
S370L	no	yes	yes	8
N400K	yes	no	yes	16
K432N	no	yes	yes	52

[a] See footnotes to Table 1.

One way to shed more light onto these issues is to estimate, using three-dimensional structures of antigen–antibody complexes and empirical free energy functions, relative contributions of individual side chains toward complex stabilities. Results obtained in this way can be compared with those derived from comparative binding data between the wild-type and mutated antigen using ELISA and immunoprecipitation assays (Webster et al., 1987; Nuss et al., 1993). In the present work, a previously described ΔG algorithm (Novotny et al., 1989; Novotny, 1991; Krystek et al., 1991, 1993) was applied to the complexes of N9 neuraminidase with NC41 Fab and NC10 Fab (N9–NC41 and N9–NC10 for short). Both the neuraminidase epitopes are located on the "upper" surface of the enzyme adjacent to the active-site pocket (Colman et al., 1989), and they are 70% overlapping (Figures 1 and 2). A total of ~19 and ~18 residues, respectively, contact NC41 and NC10, ~12 of these being common. We found concurrent trends between the effects of mutations and the calculated $\Delta G_{residue}$ values. Mutations affecting side chains for which $\Delta G_{residue} < -1$ kcal/mol markedly reduce binding, and those involving side chains for which $\Delta G_{residue} > -1$ kcal/mol have only a small effect on binding (1 kcal = 4.2 kJ). Exceptions to this trend mostly arise where multiple substitutions at the same residue cause different effects on binding. In these cases it is usually clear from the structure how this could occur.

In order to understand mechanistically some of the effects neuraminidase mutants may have on complex formation, three-dimensional structures of selected mutants (Tulip et al., 1991) were overlaid onto the wild-type neuraminidase molecule in the NC41 and NC10 complexes, and the steric and electrostatic consequences of potentially disruptive substitutions were considered. Previously, similar approaches (Bhat et al., 1990; Haneef, 1990) showed that the His–Gln exchange at position 121 of hen egg-white lysozyme would effect steric clashes, and the loss of at least two hydrogen bonds, in the lysozyme–antibody D1.3 complex, and that the lysozyme R68K mutation weakens the binding of the HyHEL-5 antibody by 1000-fold (Smith-Gill et al., 1982) because Arg 68 makes salt bridges with Glu 35 and Glu 50 on the antibody heavy chain (Sheriff et al., 1987). We observed similar types of steric and electrostatic incompatibilities with several of the neuraminidase escape mutants.

METHODS

(a) Atomic Coordinates and Structural Superpositions. The crystal structure of the N9–NC41 Fab complex was refined to an R-factor of 0.191 at 2.5-Å resolution with 56% data completeness (Tulip et al., 1992a), and the coordinates were deposited (PDB entry 1NCA). The N9–NC10 Fab complex was refined to an R-factor of 0.200 with 69% data completeness at 3.0-Å resolution (unpublished results), and the coordinates have been deposited in the PDB. The average coordinate error in the N9–NC41 complex structure is 0.3 Å,

Table 3: N9–NC41 Complex: Calculated $\Delta G_{residue}$ Contributions for the N9 Neuraminidase (kcal/mol)

residue	contact surface (Å²)	ΔG_{HB}[a]	ΔG_{EL}[b]	N (torsion)	$-T\Delta S_{CF}$[c]	total
$\Delta G < -1$ kcal residues						
Lys 463	45	−1.1	−5.5	3	1.8	−4.8
Lys 432	107	−2.7	−4.3	5	3.0	−4.0
Ala 369	73	−1.8	−1.6	0	0	−3.4
Asn 400	64	−1.6	−2.2	2	1.2	−2.6
Thr 401	134	−3.3	−0.3	2	1.2	−2.4
Arg 327	10	−0.2	−1.7	0	0	−1.9
Ile 368	60	−1.5	−1.5	2	1.2	−1.8
Pro 431	57	−1.4	0.0	0	0	−1.4
Ser 367	18	−0.4	−1.8	2	1.2	−1.0
$\Delta G > -1$ kcal residues						
Asn 329	67	−1.7	−0.3	2	1.2	−0.8
Lys 435	24	−0.6	−1.3	2	1.2	−0.7
Pro 328	24	−0.6	−0.1	0	0	−0.7
Leu 399	61	−1.5	−0.3	2	1.2	−0.6
Pro 326	20	−0.5	0.0	0	0	−0.5
Gly 343	22	−0.5	0.0	0	0	−0.5
Trp 403	43	−1.1	0.0	1	0.6	−0.5
Ser 370	19	−0.5	−1.0	2	1.2	−0.3
Asp 330	6	−0.1	0.1	0	0	−0.1
Asn 345	42	−1.0	−0.2	2	1.2	0.0
Man200D	26	−0.6	0.0	1	0.6	0.0
Asn 344	35	−0.9	−0.2	2	1.2	0.1
Man200F	10	−0.3	−0.1	1	0.6	0.2
Ile 149	13	−0.3	0.0	1	0.6	0.3
Asn 347	31	−0.8	−0.1	2	1.2	0.3
Ile 366	27	−0.7	0.0	2	1.2	0.5
Glu 465	8	−0.2	−0.2	1.5	0.9	0.5
Ser 372	11	−0.3	−0.2	2	1.2	0.7
Asp 434	52	−1.3	0.8	2	1.2	0.7
Asp 402	10	−0.3	0.6	2	1.2	1.5
Glu 433	21	−0.5	0.7	3	1.8	2.0

[a] ΔG_{HB} is −25 cal mol^{-1} Å^{-2} due to the hydrophobic effect. 1 cal = 4.18 J. [b] ΔG_{EL} is the electrostatic enthalpy change. [c] N is an estimate of the number of side-chain torsion angles frozen by the formation of the complex and leads directly to the estimated loss of conformational entropy of side chains, $-T\Delta S_{CF}$, as described in Methods.

Table 4: N9–NC41 Complex: Calculated $\Delta G_{residue}$ contributions for the NC41 Antibody Fv Fragment (kcal/mol)[a]

residue	contact surface (Å²)	ΔG_{HB}	ΔG_{EL}	N (torsion)	$-T\Delta S_{CF}$	total
Heavy Chain						
$\Delta G < -1$ kcal residues						
Glu 96	61	−1.5	−5.5	3	1.8	−5.2
Glu 56	42	−1.1	−5.0	1.5	0.9	−5.2
Asp 97	56	−1.4	−4.3	2	1.2	−4.5
Asn 31	104	−2.6	−1.6	2	1.2	−3.0
Asn 98	93	−2.3	−1.2	2	1.2	−2.3
$\Delta G > -1$ kcal residues						
Glu 61	23	−0.6	−1.2	1.5	0.9	−0.9
Phe 99	53	−1.3	0.0	1.5	0.9	−0.4
Asn 53	45	−1.1	0.7	2	1.2	0.2
Lys 64	12	−0.3	−0.4	1.5	0.9	0.2
Tyr 32	48	−1.2	0.0	2.5	1.5	0.3
Trp 50	7	−0.2	0.0	1	0.6	0.4
Thr 30	9	−0.2	0.1	1	0.6	0.5
Asn 52	18	−0.4	−0.2	2	1.2	0.6
Thr 54	9	−0.2	0.2	1	0.6	0.6
Thr 28	14	−0.4	0.0	2	1.2	0.8
Ser100A	4	−0.1	0.3	1	0.6	0.8
Leu100B	4	−0.1	0.0	1.5	0.9	0.8
Light Chain						
$\Delta G < -1$ kcal residues						
Trp 50	96	−2.4	−0.7	1	0.6	−2.5
Tyr 49	57	−1.4	−1.2	2	1.2	−1.4
$\Delta G > -1$ kcal residues						
Pro 94	51	−1.3	0.6	0	0	−0.7
Tyr 92	73	−1.8	−0.3	2.5	1.5	−0.6
Thr 53	66	−1.6	−0.1	2	1.2	−0.5
Arg 54	7	−0.2	0.0	0	0	−0.2
Ile 56	50	−1.2	0.0	2	1.2	0.0
His 91	11	−0.3	−0.3	1	0.6	0.0
Thr 31	17	−0.4	−0.1	1	0.6	0.1
Ser 93	31	−0.8	−0.3	2	1.2	0.1
Ser 52	33	−0.8	−0.1	2	1.2	0.3
Trp 96	9	−0.2	0.0	1	0.6	0.4
His 55	15	−0.4	0.0	2	1.2	0.8

[a] See footnotes to Table 3.

and that in the N9–NC10 complex is 0.4 Å, while the errors in solvated side chains in both complexes are larger (up to 1.0 Å). This level of accuracy is sufficient for assessment of the trend in solvent accessibility in both complexes and for the trend in mobility in N9–NC41. Regarding hydrogen bonds, while those observed between N9 and NC41 are fairly certain, there may be buried water molecules at the interface (not seen in electron density maps) which mediate additional hydrogen bonds. The N9–NC10 hydrogen bond assignment is tentative and included here for the purpose of comparison of trends. A detailed comparison of atomic contacts between N9–NC41 and N9–NC10 is not appropriate with the current N9–NC10 model.

The structures of five uncomplexed N9 escape mutants (Tulip et al., 1991; PDB entries 2NN9–6NN9) were refined to R-factors of between 0.160 and 0.178 against data sets which are between 56 and 73% complete to 2.2- or 2.3-Å resolution. Antibody residues are numbered as in Kabat et al. (1987) with prefixes "H" and "L" denoting heavy and light chains, respectively, and N9 neuraminidase is numbered as for neuraminidase of subtype N2 as shown in Baker et al. (1987), which in N9 involves two deletions (334, 393) and two insertions (169A, 412A–412B).

Neuraminidase mutants were superimposed onto the wild-type N9 neuraminidase using the program QUANTA (Molecular Simulations, Waltham, MA). All the main-chain atoms were least-squares superimposed. Typically, the root-mean-square shift between the mutant and wild-type backbones did not exceed 0.3 Å.

(b) CONGEN Calculations. In the treatment of Novotny et al. (1989) using CONGEN (Bruccoleri & Karplus, 1987), formation of noncovalent complexes between two rigid macromolecules is attributed to (1) the hydrophobic effect (i.e., entropy change of the system due to release of water from protein–protein contact areas) ΔG_{HB}, directly proportional to the contact area in Å² (Lee & Richards, 1971) between the two molecules (Chothia, 1974):

$$\Delta G_{HB} = -25(\text{contact area}) \quad \text{(cal)} \tag{1}$$

(1 cal = 4.2 J) and (2) electrostatic (Coulombic) interaction between the two molecules, ΔG_{EL}, empirically "screened" by an effective dielectric constant:

$$G_{EL} = \frac{Q_i Q_j}{4\epsilon\pi r}; \quad \epsilon = 4r \tag{2}$$

(Q_{ij}, partial atomic charges; r, distance between the ith and jth atoms; ϵ, the effective dielectric constant). Hydrogen bonding is treated as a solely electrostatic phenomenon. These, usually attractive, interactions are counteracted by a loss of conformational entropy of surface side chains immobilized at the contact surface:

$$-T\Delta S_{CF} = NRT \log 3 = 0.6N \quad \text{(kcal)} \tag{3}$$

Equation 3 implies that each torsion has approximately three equienergetic states available in free solution (i.e., *trans* and

±gauche) but becomes locked in one conformation upon the formation of a complex (hence the log 1/3 = –log 3 term) (R, the gas constant; T, temperature, = 300 K; N, number of side-chain torsional degrees of freedom lost). Polar hydrogen atoms placed by CONGEN are considered parts of distinct torsions, but other hydrogen atoms are not. The criterion for counting N is based on the atoms which have surface area buried by the interaction, and the size and context of the side chain are taken into account (hence the noninteger values of N for some side chains). For instance, Trp side chains were assigned N = 1 because they have been shown experimentally to possess freedom to move in the docking process (Arevalo et al., 1993; Padlan et al., 1989).

The CONGEN program was used to calculate the pairwise electrostatic interactions of all the atoms in the system (eq 2) and the atomic solvent accessibilities (eq 1). The data were automatically assembled into difference tables collating atomic electrostatic energy differences and atomic contact surfaces. The solvent accessibility tables were used to estimate the number of torsional degrees of freedom lost upon complex formation (eq 3). These atomic contributions were then added to obtain sums for each residue ($\Delta G_{residue}$) as well as for the individual molecules.

As the focus of the current work is on the calculated $\Delta G_{residue}$ and, implicitly, the $\Delta\Delta G$ values (i.e., differences between the wild-type and mutant free energy changes, ΔG), contributions from cratic and translational/rotational entropy changes to the overall free energy change of complex formation are unimportant. For the absolute ΔG value calculations, however, such as those reported previously and briefly mentioned here, the cratic and translational/rotational entropy changes were estimated to be ≈11 kcal (Novotny et al., 1989).

All calculations are based on one subunit of neuraminidase in complex with the Fv fragment of the antibody. Included are the three terminal sugar residues in the carbohydrate attached to the Asn 200 of a neighboring neuraminidase subunit (three mannose residues labeled 200D, 200E, and 200F). No explicit water molecules were present in our calculations. In CONGEN, 200 cycles of the adopted-base Newton–Raphson (ABNR) energy minimization were applied to the crystal structures before evaluating components of the free energy. The purpose of the minimization was to adjust the X-ray crystallographic coordinates to the force-field parameters used, and in order to minimize excessive movements away from the coordinates, harmonic constraints of 20 kcal/atom were applied on the current atomic positions (Novotny et al., 1989). The root-mean-square shifts between the starting and final structures were small, 0.3 Å for the VL domain, VH domain, and the neuraminidase, respectively, and commensurate with the crystallographic resolutions of the two complexes. Still, interactions between charge-alike groups in the X-ray structure are somewhat downweighted here, and charge-different interactions are enhanced: for example, the distance of the salt bridge between Lys 432 on neuraminidase and Asp H97 on NC41 was reduced by 0.4 Å, i.e., from 3.6 to 3.2 Å.

Large probe accessibility calculations were carried out as described by Novotny et al. (1986). The Lee and Richards (1971) accessibility algorithm, as implemented in the program CONGEN, was used to identify neuraminidase surface areas that come in contact with a spherical probe, 10-Å radius, with protein residues from a neighboring neuraminidase subunit included for collision purposes. The accessible contact surface data obtained in this way were smoothed by a seven-residue moving window algorithm (Novotny et al., 1986).

RESULTS

(a) Experimental Binding Data. The dissociation constant (K_D) between tern N9 neuraminidase and NC41 Fab is 8.3 × 10^{-8} M (ΔG = –9.7 kcal/mol; Gruen et al., 1993) as measured using an air ultracentrifuge and radioactive iodination of tyrosine residues. The K_D between tern N9 neuraminidase and NC10 Fab is 1.4 × 10^{-8} M (ΔG = –10.8 kcal/mol; Gruen et al., 1993). Tables 1 and 2 contain binding data from ELISA and immunoprecipitate assays (Nuss et al., 1993; Webster et al., 1987) showing which mutations cause a marked reduction relative to wild-type tern N9 neuraminidase in binding to NC41 and NC10. The quantitative decrease in binding affinity for each mutant remains to be experimentally determined. The apparent binding energies from mutagenesis experiments, i.e., $\Delta\Delta G$ values, are measurements of specificity of binding and usually cannot be equated with true binding energies (Fersht, 1988).

(b) Calculated $\Delta G_{residue}$ Values: Correspondence with Mutant Binding Data. The goal of our present calculations is to discriminate, on a coarse level, those residues which most determine specificity from those which are more passive. The simplifications of the empirical free energy method as discussed, e.g., by us (Krystek et al., 1993) and others (Janin & Chothia, 1990; Nicholls et al., 1991; Wilson et al., 1991; Williams et al., 1991; Horton & Lewis, 1992; Privalov & Makhatadze, 1993; Murphy et al., 1993; Pickett & Sternberg, 1993; Sternberg & Chickos, 1994) require that the results not be interpreted too finely or as absolute values. Calculations described in this paper will hopefully point the way toward further refinement of the individual terms of the formula, with a promise of an improved algorithm in the future. For example, the energy of solvated salt bridges appears to be overestimated because the effective dielectric constant used here, $\epsilon = 4r$, accounts for the solvent shielding only in an approximate way. The problem is particularly bad for the N9–NC41 complex where highly favorable ΔG values are calculated for the solvated salt bridge between Lys 463 (–4.8 kcal) and Glu H56 (–5.2 kcal). It is likely that mutation of either residue would have only a small effect on the binding affinity (<15 fold, <1.5 kcal), consistent with mutations of solvated salt bridges in protein folding (Dao-pin et al., 1991). Thus, although the overall ΔG for the N9–NC10 complex was well approximated by the calculations (–10.8 kcal/mol experimental, –12.6 kcal/mol calculated), that for the N9–NC41 complex was overestimated by about 130% (–9.7 kcal/mol experimental, –22.4 kcal/mol calculated).

Tables 3 and 4 list the $\Delta G_{residue}$ values of residues in N9 and NC41 ranked from most negative to most positive and partitioned into two groups with $\Delta G_{residue}$ = –1 kcal/mol as the dividing point. Tables 5 and 6 show the corresponding lists of residues for the N9–NC10 complex. Several interesting trends emerge from Tables 1 and 2 (i.e., comparison of calculations with the experiment).

(i) A relatively small group of neuraminidase residues is predicted to have large negative $\Delta G_{residue}$ values due to salt bridges and favorable hydrogen bonds, and the remaining residues are either energetically neutral or in a few cases repulsive. In the N9–NC41 complex, the buried salt bridge between Lys 432 (–4.0 kcal) and Asp H97 (–4.5 kcal) is very favorable while the three intermolecular hydrogen bonds formed by Glu H96 (–5.2 kcal) give it the most negative $\Delta G_{residue}$ value. The energies of the salt bridges, particularly the highly solvated salt bridge between Lys 463 (–4.8 kcal) and Glu H56 (–5.2 kcal), are probably overestimated here for reasons discussed above. Other uncharged residues in the

Table 5: N9–NC10 Complex: Calculated $\Delta G_{residue}$ Contributions for the N9 Neuraminidase (kcal/mol)[a]

residue	contact surface (Å²)	ΔG_{HB}	ΔG_{EL}	N (torsion)	$-T\Delta S_{CF}$	total
$\Delta G < -1$ kcal residues						
Lys 432	41	−1.0	−5.0	4	2.4	−3.6
Asn 329	85	−2.1	−1.9	3	1.8	−2.2
Man200F	54	−1.3	−1.3	1	0.6	−2.0
Ala 369	55	−1.4	−0.2	0	0	−1.6
Thr 401	48	−1.2	−0.9	1	0.6	−1.5
Pro 328	37	−0.9	−0.4	0	0	−1.3
Gly 343	43	−1.1	0.1	0	0	−1.0
Ser 370	18	−0.5	−1.7	2	1.2	−1.0
$\Delta G > -1$ kcal residues						
Pro 331	26	−0.6	0.0	0	0	−0.6
Pro 342	24	−0.6	0.0	0	0	−0.6
Trp 403	47	−1.2	0.0	1	0.6	−0.6
Man200E	27	−0.7	0.1	0	0	−0.6
Man200D	19	−0.5	0.0	0	0	−0.5
Ile 368	58	−1.5	0.0	2	1.2	−0.3
Asn 400	72	−1.8	−0.2	3	1.8	−0.2
Thr 332	40	−1.0	−0.2	2	1.2	0.0
Lys 336	13	−0.3	−1.5	3	1.8	0.0
Ile 366	19	−0.5	0.0	1	0.6	0.1
Val 333	16	−0.4	0.0	1	0.6	0.2
Ser 367	28	−0.7	−0.3	2	1.2	0.2
Asp 330	17	−0.4	0.7	0	0	0.3
Asn 344	31	−0.8	−0.1	3	1.8	0.9
Tyr 341	29	−0.7	0.0	3	1.8	1.1
Ser 372	5	−0.1	0.0	2	1.2	1.1

[a] See footnotes to Table 3.

Table 6: N9–NC10 Complex: Calculated $\Delta G_{residue}$ Contributions for the NC10 Antibody Fv Fragment (kcal/mol)[a]

residue	contact surface (Å²)	ΔG_{HB}	ΔG_{EL}	N (torsion)	$-T\Delta S_{CF}$	total
Heavy Chain						
$\Delta G < -1$ kcal residues						
Asp 56	69	−1.7	−6.5	2	1.2	−7.0
Asn 54	82	−2.0	−1.2	3	1.8	−1.4
Tyr 99	97	−2.4	−0.1	2	1.2	−1.3
$\Delta G > -1$ kcal residues						
Tyr100A	60	−1.5	−0.5	2	1.2	−0.8
Asp100B	21	−0.5	−1.5	2	1.2	−0.8
Gly 53	16	−0.4	0.1	0	0	−0.3
Gly 55	9	−0.2	0.0	0	0	−0.2
Tyr 57	11	−0.3	−0.5	1	0.6	−0.2
Tyr 52	30	−0.8	−0.2	2	1.2	0.2
Ser 58	9	−0.2	−0.2	2	1.2	0.8
Arg 100	74	−1.9	0.2	5	3.0	1.3
Light Chain						
$\Delta G < -1$ kcal residues						
Phe 92	88	−2.2	−1.1	2	1.2	−2.1
Asp 91	3	−0.1	−1.4	0	0	−1.5
$\Delta G > -1$ kcal residues						
Asp 28	44	−1.1	−1.0	2	1.2	−0.9
Gln 27	37	−0.9	−0.1	1	0.6	−0.4
Thr 93	57	−1.4	0.1	2	1.2	−0.1
Ser 30	45	−1.1	−0.1	2	1.2	0.0
Leu 94	54	−1.3	0.1	2	1.2	0.0
Tyr 50	9	−0.2	0.0	1	0.6	0.4
Tyr 32	52	−1.3	0.4	3	1.8	0.9
Asn 31	14	−0.3	0.1	2	1.2	1.0

[a] See footnotes to Table 3.

group make favorable hydrogen bonds and/or have large buried surface area. On N9, Thr 401 (−2.4 kcal) has the largest single buried surface area (134 Å²) and makes one hydrogen bond, and Ala 369 (−3.4 kcal) has a large buried surface (73 Å²) and makes two hydrogen bonds, while on NC41, Trp L50 (−2.5 kcal) has 96 Å² of buried surface and makes one hydrogen bond. Excluding Lys 463, eight $\Delta G <$ −1 kcal/mol residues are spread over four contact segments in the epitope, and they occur in three clumps. The results show that CDR loop H3 is dominant but that $\Delta G < -1$ kcal/mol residues are present in the H1 and L2 loops as well. The H3 loop may have undergone conformational changes in binding which would downweight the calculated ΔG values shown here.

In the N9–NC10 complex, similarly to N9–NC41, a salt bridge between Lys 432 (−3.6 kcal) and Asp H56 (−7.0 kcal) is prevalent, although its energy is likely to be overestimated here. On the antigen, Asn 329 makes a major contribution due to having a large buried surface (85 Å²) and three hydrogen bonds; a fully buried carbohydrate residue, Man 200F, also features highly. There are no torsional angles and hence no loss of conformational entropy for three of the $\Delta G < -1$ kcal/mol residues, Ala 369, Pro 328, and Gly 343. The eight $\Delta G < -1$ kcal/mol residues are spread over the surface with at least one residue lying in each of the six epitope segments, five of the eight residues occurring in clumps. On the antibody, the $\Delta G < -1$ kcal/mol residues Asn H54, Asp L91, and Phe L92 make one hydrogen bond each. In contrast with N9–NC41, residues from CDR H2 and CDR L3, not from CDR H3, have the strongest interaction with the neuraminidase.

(ii) Mutants with substitutions at sites for which $\Delta G < -1$ kcal/mol do not bind the antibody while mutants with substitutions at sites where $\Delta G > -1$ kcal/mol do bind. Tested against binding data reported by Nuss et al. (1993) and Webster et al. (1987), the trend is valid for NC41 in 19 out of 27 cases at 13 neuraminidase sites (i.e., by comparison of columns 2 and 3 in Table 1), and it is valid for NC10 in 7 out of 7 cases at 7 neuraminidase sites (columns 2 and 3 in Table 2). The value of −1 kcal/mol was chosen as the point which best separates the binding from the nonbinding mutants in Tables 3 and 5. We do not attribute much significance to the absolute value of this point, although we note that it is roughly commensurate with energetic threshold of thermal (Brownian) noise at room temperature (1 kT or 0.6 kcal). Most of the $\Delta G < -1$ kcal/mol residues are involved in hydrogen bonds and/or salt bridges with the antibody. Consequently, the corresponding trend linking the binding data with the presence of these interactions is almost as good as that mentioned above: 18 out of 27 for NC41 (columns 2 and 4 in Table 1) and, tentatively, 5 out of 7 for NC10 (columns 2 and 4 in Table 2). Since most of these electrostatic interactions in the interfaces are not accessible to solvent, this is in accord with the destabilization of protein folding caused by mutation of side chains involved in buried hydrogen bonds (Alber et al., 1987a) or partially buried salt bridges (Anderson et al., 1990).

(iii) Considering the N9–NC41 complex, some of the successful predictions are notable [historically, the CONGEN calculations were done before the mutant binding data of Nuss et al. (1993) were available]. All mutations at the buried residues Ser 367 and Asn 400 markedly reduce binding as predicted by the trend. Asn 329 lies at the periphery of the interface and is predicted to be nonenergetic, in accord with the fact that substitution by either Asp or Lys does not markedly reduce binding. Lys 432, also near the periphery, is predicted to be energetic because it makes a critical salt bridge with NC41, and replacement of Lys 432 by Asn or Asp does markedly reduce binding. Although the N344I mutant disrupts a hydrogen bond, it retains binding, as predicted by CONGEN.

(iv) Regarding the N9–NC10 complex, all seven mutations for which we have binding data follow the trend. Remarkably, the positive binding result of the I368R mutant agrees with

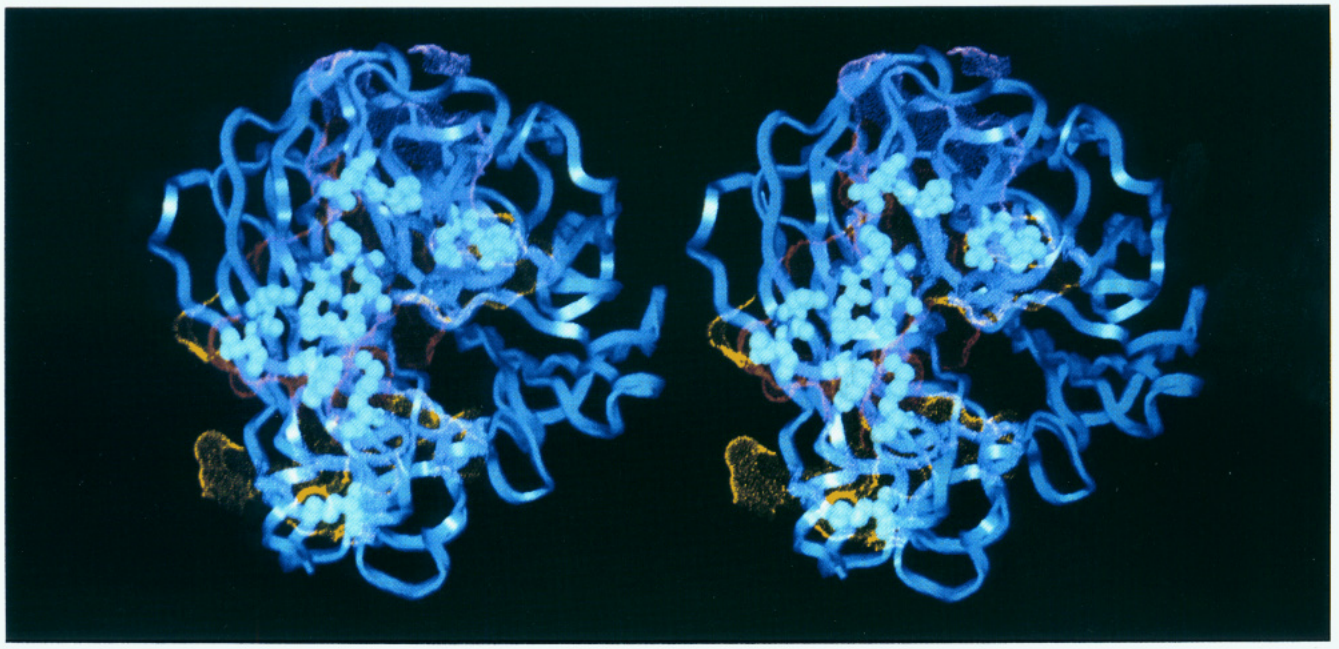

FIGURE 1: Antigenic epitopes and mutated side chains. In this regular (as opposed to cross-eye) stereo diagram, the N9 neuraminidase polypeptide chain is shown as a blue ribbon, and non-hydrogen atoms of the side chains are shown as cyan spheres. The NC41 and NC10 antigenic epitopes are depicted as the Connolly (1983) dot rendering of the Lee and Richards (1971) solvent-accessible surface. Color coding of the surfaces is as follows: red, overlap epitopic surface common to both the NC41 and NC10 antibodies; yellow-brown, epitopic surface unique to the NC41 antibody; magenta, epitopic surface unique to the NC10 antibody.

the trend even though Ile 368 lies at the spatial center of the epitope. Similarly to NC41, Lys 432 is at the edge of the interface, but it makes a critical salt bridge which gives it a favorable $\Delta G_{residue}$, and replacement by Asn markedly reduces binding.

(v) Exceptions to the trend involving $\Delta G_{residue}$ values for N9–NC41 are labeled I–V in Table 1: (I) in the I368R and I368Y mutants the main ΔG contribution from residue 368 is due to a hydrogen bond from the backbone nitrogen to Glu H96, while the Ile side chain is energetically noncritical and lies at the bottom of a solvent-accessible pocket, thus allowing the mutations to larger residues, and in the I368R mutant there is a conformational change (Tulip et al., 1992b); (II) in the A369G mutation a smaller residue does not upset shape complementarity or remove a critical hydrogen bond; (III) in the S370L, S372Y, and S372F mutants the small side chains, although not in critical contacts, are nevertheless in solvent-inaccessible positions so that a mutation to a larger side chain disrupts the shape complementarity; (IV) in the T401L mutant we cannot explain from the crystal structure how Leu could be accommodated at residue 401 which is not mobile and is closely packed against, and almost entirely buried by, NC41 Fab; (V) K432R, a conservative substitution, apparently does not upset the critical salt bridge. Thus reasonable explanations for all but one of the exceptions (T401L) are evident from the N9–NC41 crystal structure. Five out of eight exceptions in the trend (A369G, S370L, S372Y, S372F, and K432R) occur where mutations toward smaller and larger residues, respectively, produce different effects on binding.

(vi) Given the fact that ≈70% of the NC41 and NC10 epitopes overlap, one might expect approximately two-thirds to three-quarters of the $\Delta G_{residue} < -1$ kcal neuraminidase side chains in the two complexes, as listed in Tables 3 and 5, to be identical. Moreover, the $\Delta G < -1$ kcal residues from the overlap area (i.e., common to both the NC10 and NC41 epitopes) may be expected to contribute comparable binding energies to the two complexes. This is clearly not the case, however, and the two antibodies, NC41 and NC10, can be said to recognize an identical neuraminidase surface patch in different ways. A contrasting situation has been found in protease–protein inhibitor association where, in several different complexes (e.g., chymotrypsin and *Staphylococcus aureus* protease B in complex with the turkey ovomucoid third domain), the binding energy attribution was found to be very similar (Krystek et al., 1993).

(c) Comparison with Experimentally Determined Functional Epitopes. Nuss et al. (1993) systematically made substitutions to residues in the N9–NC41 epitope and then assayed the effects on antibody binding. Their conclusion that only several (Ser 367, Asn 400, and Lys 432) of the epitope residues contacting the antibody were critical for binding is in agreement with this study, although a larger group of "energetic" residues is suggested by the CONGEN calculations, 9 residues for N9–NC41 (19 are in contact with the antibody) and 8 for N9–NC10 (18 residues contact NC10). The size of the functional epitope depends somewhat on the criterion used for its definition, and it is not yet possible to compare binding data from the neuraminidase and growth hormone systems. Jin et al. (1992) found that, per epitope, the numbers of alanine substitutions causing a >2-fold or >20-fold effect upon binding affinity are on average eight (range 4–14) and three (range 1–7), respectively, which is more in accordance with Nuss et al. (1993) than with the CONGEN results. Part of the discrepancy may arise because the large negative $\Delta G_{residue}$ values of some residues in the CONGEN functional epitopes are due to favorable contacts made by main-chain atoms only (Arg327 in N9–NC41) and can be "invisible" to mutagenesis (Smith & Benjamin, 1991).

Charged residues, two and three for N9 and NC41, respectively, and one and two for N9 and NC10, feature highly on the lists of $\Delta G_{residue} < -1$ kcal/mol side chains (Tables 3–6), although we discussed previously the uncertainties of the $\Delta G_{residue}$ contributions of charged residues. Jin et al. (1992) reported that charged residues play a prominent role in most functional epitopes and that out of the average number of eight residues causing >2-fold reduction in affinity, on average

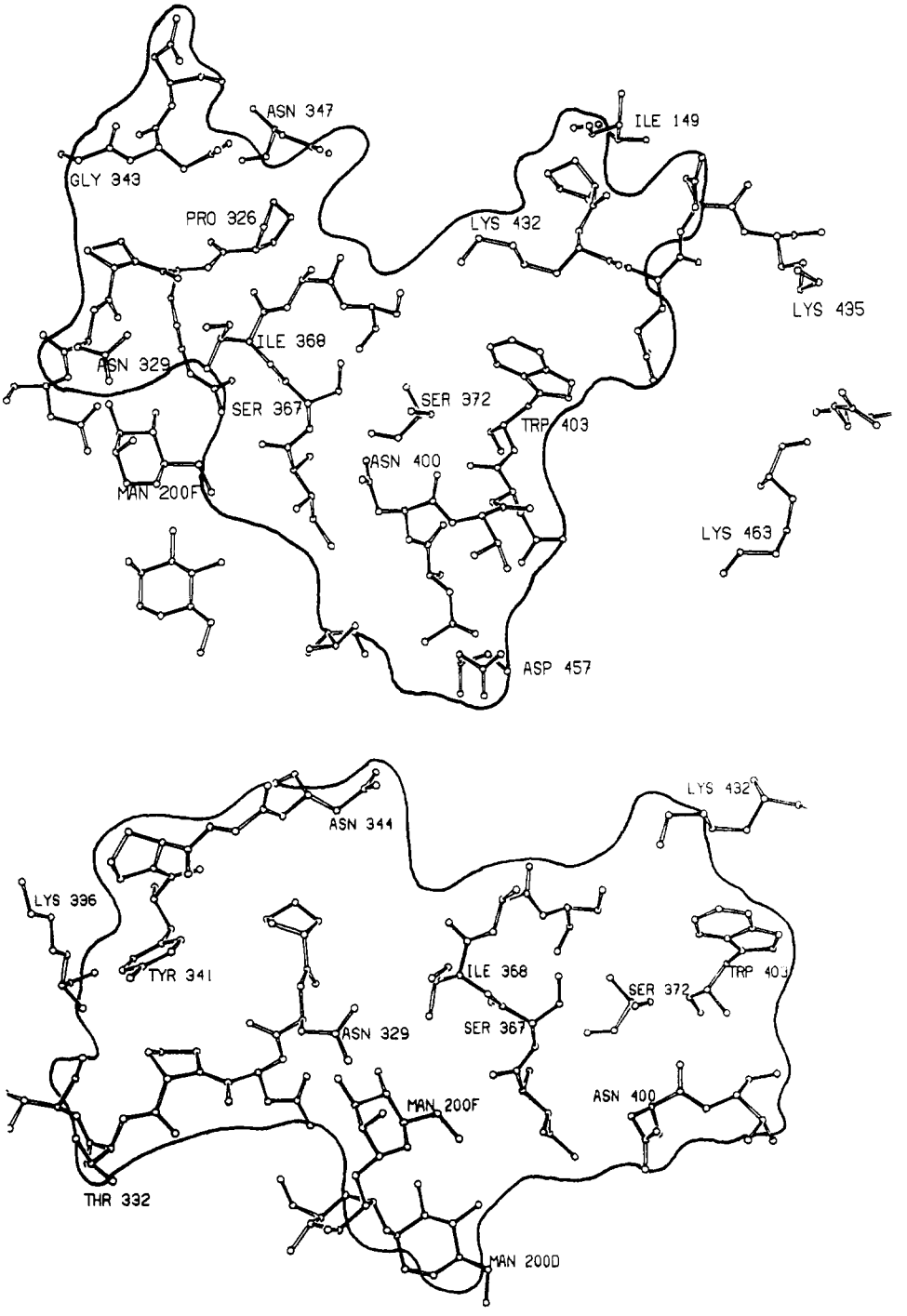

FIGURE 2: Epitope regions of (A, top) N9–NC41 and (B, bottom) N9–NC10, including all neuraminidase residues with buried surface (>4 Å^2). The thick line surrounding each epitope roughly indicates the periphery of the buried surface of the main contact region calculated before energy minimization in CONGEN.

2.8 are charged. In contrast with the findings of Jin et al. (1992), Lys dominates the predicted N9 functional epitopes rather than Arg, which may simply reflect the coincidence of particular Lys and Arg residues with antigenic regions in N9 and the growth hormone, respectively. The predicted energetic residues are spread over different segments and different regions of the epitope in both the N9–NC41 and N9–NC10 complexes. Accordingly, the functional epitopes on the growth hormone are mostly discontinuous (Jin et al., 1992), and the maximum average distance between disruptive alanine sites is 20 Å.

(d) Properties of Wild-Type Residues, Complexed and Uncomplexed. Tables 1 and 2 contain structural information about each of the mutation sites which lie in the epitopes recognized by NC41 and NC10, respectively, including solvent-accessible surface areas in the complexed and uncomplexed crystal structure and average main-chain temperature factors (in the N9–NC41 complex only). Figure 1 shows a ribbon trace of one subunit of neuraminidase along with the buried Connolly surface of each epitope and the mutated residues. Figure 2 displays all the residues lying in the epitopes of the N9–NC41 and N9–NC10 complexes marked with the periphery of each epitope.

Solvent Accessibility. Table 1 and Figure 2A indicate that most of the small-to-large mutations which disrupt binding of NC41 are central in the epitope of the N9–NC41 complex. S367N, A369D, S370L, S372Y, and N400Q, which do not bind NC41, have zero or small solvent accessibilities in the

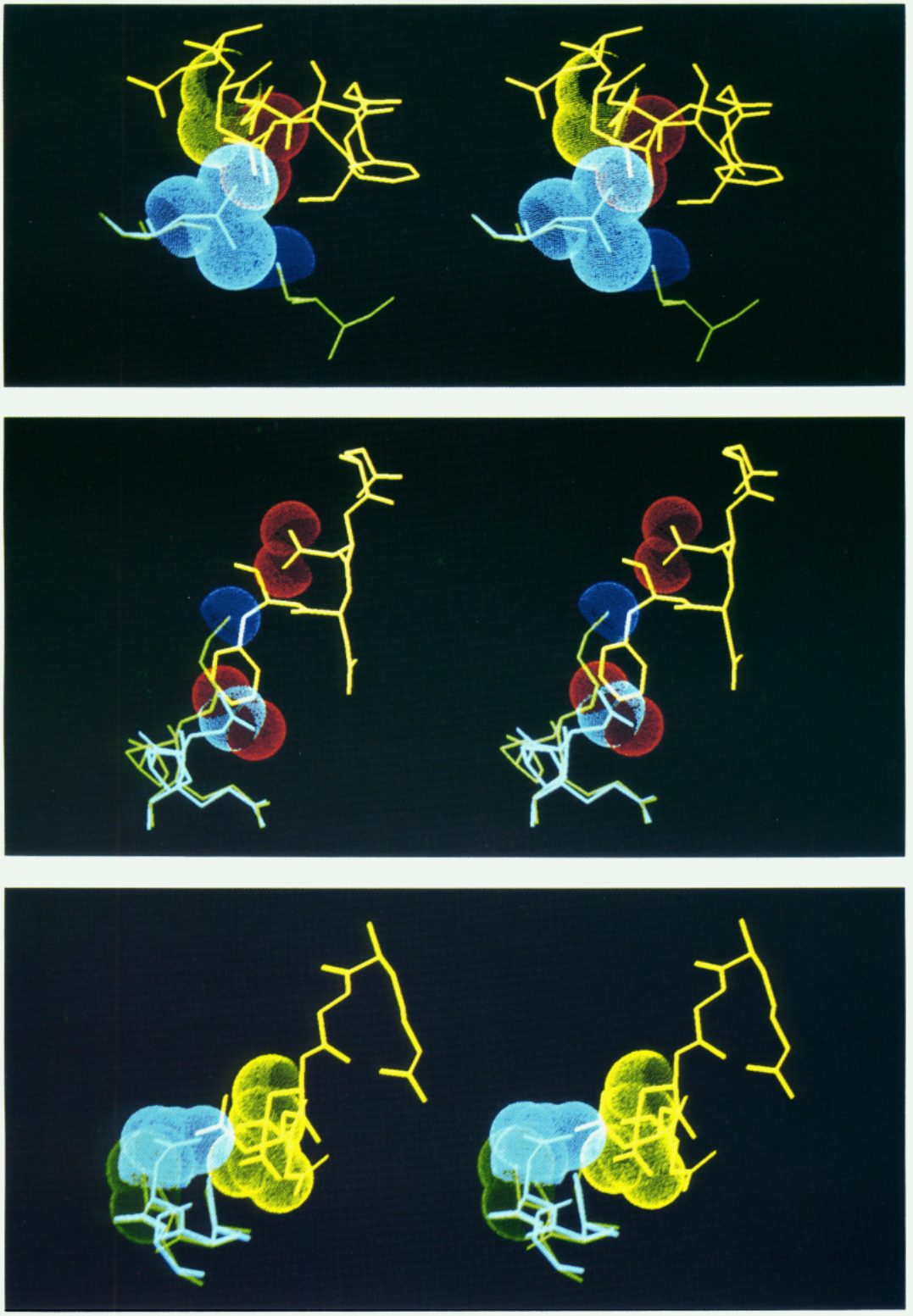

FIGURE 3: X-ray crystallographic structures of various uncomplexed mutants overlaid onto the crystal structure of the neuraminidase in the NC41 antibody complex. In what follows, the wild-type N9 neuraminidase polypeptide chain is color-coded green, that of the N9 mutants is cyan, and the antibody heavy chain is yellow. (A, top) Docking of the S370L mutant: no observed binding. The Leu 370 mutant side chain (cyan spheres) disrupts shape complementarity (wt Ser 370–Asp H97, 2.7 Å; mutant Leu 370–Asp H97, 0.9 Å) and a buried salt link between the antibody Asp H97 (CG and CD atoms, yellow; OE1 and OE2 atoms, red) and the N9 Lys 432 (the terminal nitrogen, blue). (B, middle) Docking of the K432N mutant: no observed binding. The substitution is effectively a reduction in size and does not cause a steric clash but involves the loss of the Lys 432–Asp H97 buried salt link (the Lys 432 terminal nitrogen, blue; the Asn 432 CG atom, cyan, and the OD1 and ND2 atoms, red; the Asp H97 OD1 and OD2 atoms, red). (C, bottom) Docking of the A369D mutant: no observed binding. The stereo diagram shows a comparison of the Ala 369 (green dot spheres) and the Asp 369 side chains. A steric and electrostatic clash between the N9 mutant Asp side chain and the antibody Glu H97 (yellow spheres) is apparent (wt Ala 369–Glu H96, 4.0 Å; mutant Asp 369–Glu H96, 2.2 Å).

wild-type complex, while P328K, N329K, and I368R (picking only one such mutation at each site) are near/directed toward the periphery and retain binding to NC41. In the NC10 complex, however (Table 2, Figure 2B), the trend is valid in two out of six cases. I368R, for example, lies in the center of the epitope (Figure 2B), and the Arg side chain is apparently

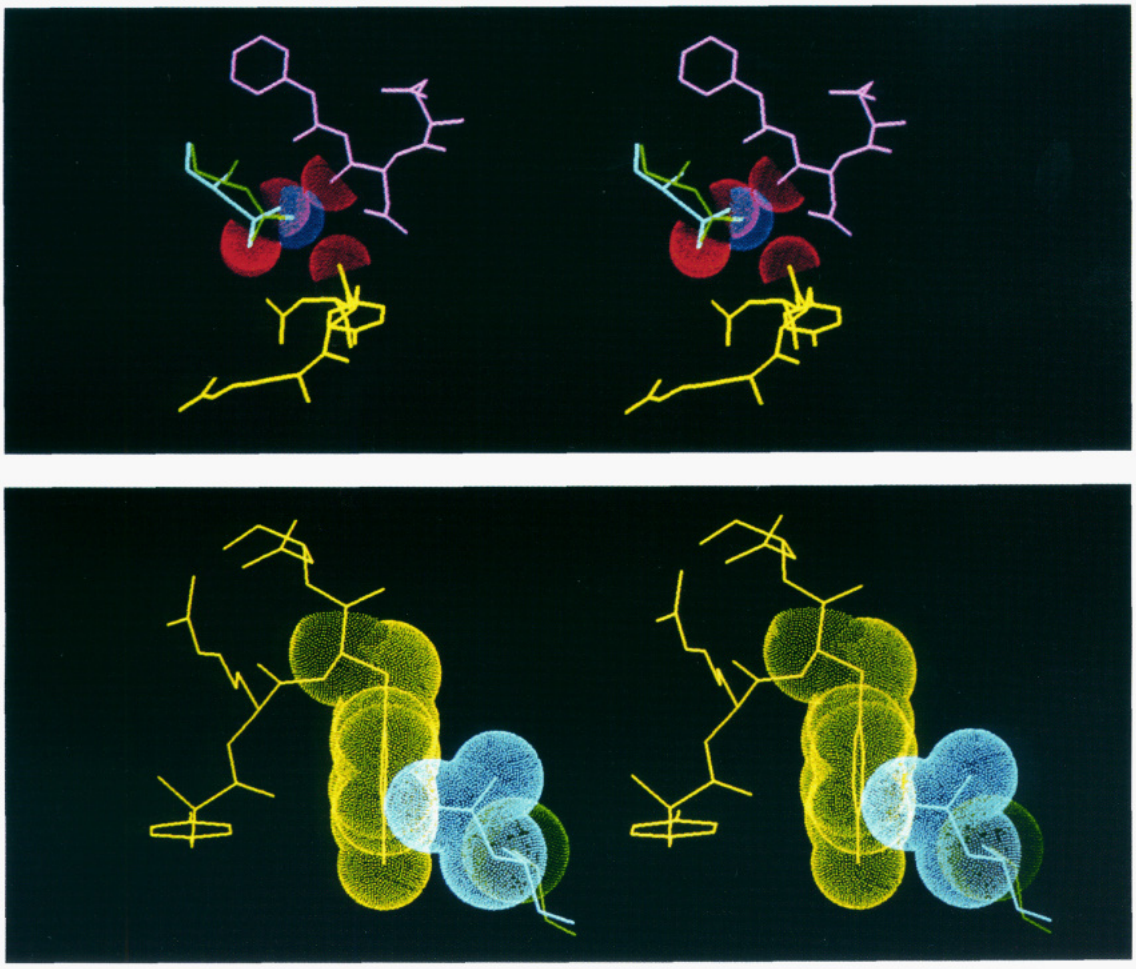

FIGURE 4: X-ray crystallographic structures of various uncomplexed mutants overlaid onto the crystal structure of the neuraminidase in the NC10 antibody complex. In what follows, the wild-type N9 neuraminidase polypeptide chain is color-coded green, that of the N9 mutants is cyan, the antibody heavy chain is yellow, and the antibody light chain is magenta. (A, top) Docking of the N329D mutant: no observed binding. As shown in the stereo diagram, a replacement of Asn 392 by Asp (on the left; the Asp terminal oxygen atoms are shown in red and the Asn terminal oxygen and amide nitrogen atoms are in red and blue, respectively) would cause two hydrogen bonds to be lost to main-chain oxygen atoms (shown as red spheres) of Asp L91 and Tyr H100A. (B, bottom) Docking of the A369D mutant: no observed binding. There would be a steric clash between Asp 369 (cyan) and the side chain of Tyr H100A (yellow); (the wild-type Ala is shown in green) (wt Ala 369–Tyr H100A, 4.1 Å; mutant Asp 369–Tyr H100A, 1.4 Å).

accommodated in space which in the wild-type complex is a cavity. It may be that cavity accessibility is as important as accessibility to bulk solvent. The trend for N9–NC41 is in accordance with functional studies of Wells (1991), who compared the high-resolution epitope mapping of four proteins and found that the dominant functional effects tend to cluster near the center of a patch of residues, with weaker effects toward the periphery.

Mobility. The trend for N9–NC41 is for highly destabilizing mutations to be at rigid residues in the complex, just as protein folding is more destabilized by mutations at rigid residues in the core than by mutations at mobile residues (Alber et al., 1987b). The average temperature factor of all neuraminidase residues in the N9–NC41 complex is 9.9 Å^2. If mobile residues are defined as those with the average main-chain temperature factor greater than 15 Å^2 in the complex (i.e., 1.5 times the global average), then all mutations occurring in the 320–350 loop lie at mobile residues in the complex and are binders. Residues in the 366–372 loop are mostly not mobile, and the small-to-large mutations do not bind (except those at 368 as explained above). Residues in the 399–403 loop are not mobile, too, and the three binding results for the small-to-large mutations are varied (two do not bind, one does bind). In the 431–435 loop, Lys 432 appears to become considerably less mobile when it forms a salt bridge upon formation of a complex and K432N does not bind. The trend is much less closely followed for mobilities in the uncomplexed structure.

Turner et al. (1992) reported a similar trend for mutations lying in the $\alpha_1\beta_2$ interface of deoxy- and oxyhemoglobin. The binding affinity of proteinase inhibitors is very sensitive to mutations in the binding loop (Laskowski et al., 1989) which is held rigid in the complexed state (Bode & Huber, 1991). A concurrent observation was made (Novotny et al., 1989); Novotny, 1991) for the D1.3, HyHEL-5, and HyHEL-10 antibodies, namely, that the energetically most important residues are located near the bottom recesses of the antigen-combining site and not the tips of the CDR loops.

Surface Protrusion (Large Probe Accessibility). Figure 5 shows the large probe contact surface profile of the N9 neuraminidase structure, together with locations of the $\Delta G <$ −1 kcal/mol residues in the NC41 and NC10 epitopes, as listed in Tables 3 and 5. All these residues are seen to cluster around positions prominently accessible to a large probe although they do not always coincide with the most protruding positions. This trend is similar to observations made earlier (Novotny et al., 1989; Novotny, 1991) for the lysozyme D1.3, HyHEL-5, and HyHEL-10 epitopes and supports the findings of Jin et al. (1992), who found a high correlation between

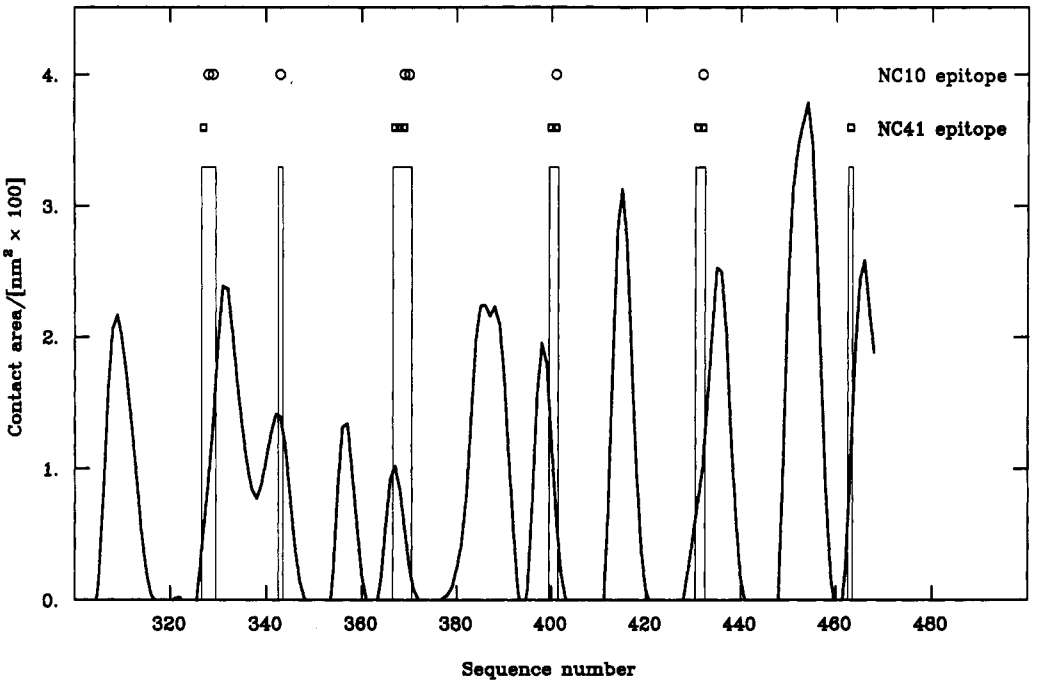

FIGURE 5: Large probe (r = 10 Å) accessibility profile of the N9 neuraminidase. The calculated residue contact areas were smoothed by three passes of the seven-residue moving window algorithm and scaled by a factor of 0.6 for visual convenience. Positions of the CONGEN-calculated attractive residues of the NC41 and NC10 energetic epitopes, as listed in Tables 3 and 5, are indicated by open squares and circles, respectively, and emphasized by vertical bars. Note that all the bars fall within the most accessible surface regions and are always in close proximity of, or coincide with, the contact area peaks.

antigenicity and large probe accessibility in the human growth hormone.

(e) Docking Pictures. In the five crystal structures of N9 escape mutants, N329D, I368R, A369D, S370L, and K432N, only local structural changes occur as a result of the mutations (Tulip et al., 1991). In the two cases of mutants still binding to NC41 (Tulip et al., 1992b) the binding of the antibody to each mutant is isosteric to that of wild-type N9. Therefore, to understand the effects of mutants which do not bind either NC41 or NC10, we examined the immediate vicinity of the site of mutation with the mutant docked to the antibody as for wild type. Figures 3 and 4 show the crystal structures of various uncomplexed mutants overlaid on the crystal structures of the neuraminidase in the N9–NC41 and N9–NC10 complexes and clearly show nonallowable substitutions in antigen–antibody interfaces. As details of particular interactions are discussed in the figure captions, only a few general comments are offered here.

First, a small-to-large mutation causing a steric repulsion is illustrated by S370L to NC41 (Figure 3A). Second, the K432N replacement in both NC41 (not shown) and NC10 (Figure 3B) is paradigmatic of a mutation which changes the formal charge of the side chain, reducing Coulombic attraction and making the energy penalty of charge desolvation prohibitive (Yang et al., 1992; Novotny & Sharp, 1992). Finally, A369D to NC41 shows both steric and electrostatic incompatibilities (Figure 3C).

While Figures 3 and 4 show the mutated side chains as they occur in the uncomplexed crystal structures, conformational changes do in fact occur in the mutated side chains of I368R and N329D docking to NC41 (Tulip et al., 1992b). Little is known about the detailed motions of side chains in the docking process. The mutant side chains appear localized in the uncomplexed crystal structures albeit with above-average temperature factors.

DISCUSSION

Results of calculations reported here give further support to the notion of a functional ("energetic") epitope (Novotny et al., 1989; Novotny, 1991; Jin et al., 1992; Nuss et al., 1993). A relatively small number of amino acids contribute actively to binding energetics and specificity; they form a subset of the total antigen–antibody contact surface. The concept previously offered a resolution of an apparent paradox: on one hand, a multitude of side-chain/side-chain interactions at the interface and, on the other hand, the experimentally documented importance of a relatively small subset of those side chains (Novotny et al., 1989; Smith-Gill et al., 1982). Experimental data consistent with the hypothesis of a functional epitope include those obtained on the human growth hormone (Cunningham et al., 1990; Jin et al., 1992; Cunningham & Wells, 1993), the human placental lactogen (Lowman et al., 1991), the λ repressor (Breyer & Sauer, 1989), and the N9 neuraminidase (Nuss et al., 1993). In addition, the calculated $\Delta G_{residue}$ values suggest that the main chain and carbohydrate can be energetically important.

Cumulative evidence from X-ray crystallography, mutant binding data, and the calculated $\Delta G_{residue}$ contributions suggests that the NC41 and NC10 antibodies recognize essentially the same area of the N9 neuraminidase surface, yet with different specificities. A new immunological dilemma thus emerges: is a unique area of protein molecular surface a single antigenic epitope or, rather, is it a multitude of different overlapping epitopes? One possible solution we may offer to this dilemma invokes the fact that the functional epitopes reside in the most protruding parts of the surface [cf. Figure 5 of this paper and also Novotny (1991), Jin et al. (1992), and Getzoff et al. (1988)]. Thus, surface antigenicity may be primarily determined by its protrusion index and presence of charged and strongly polar side chains, rather than the atomic detail relating to relative constellation of nitrogen and oxygen atoms. In this regard, the clumping of $\Delta G_{residue} < -1$ kcal/

mol side chains within different segments, the surface roughness (Lewis & Rees, 1985), and the surface curvature (Nicholls et al., 1991) of these regions merit further investigation.

This study demonstrates that avoidance of unpaired charges and unfavorable steric interactions between antigen and antibody is an important determinant of specificity as shown previously for Fab D1.3 lysozyme (Bhat et al., 1990) and for enzyme–substrate interactions (Fersht et al., 1985; Estell et al., 1986). Consequently, in many cases, highly destabilizing mutations occur at residues which are buried and relatively rigid in the complex and/or make critical intermolecular electrostatic interactions. These properties often occur together, making it difficult to factor out the causes of the marked decrease in binding of a mutant. Moreover, these trends are dependent on the structural context (e.g., cavities, side-chain direction, main-chain interactions, conformational changes). Nevertheless, docking pictures do suggest rationalizations for some data, and the $\Delta G_{residue}$ values calculated in CONGEN correspond well with the effects of mutations.

ACKNOWLEDGMENT

We thank P. M. Colman, J. N. Varghese, P. A. Tulloch, R. L. Malby, P. C. Davis, and M. C. Lawrence for helpful discussions, providing facilities, and computational assistance. We are grateful to J. M. Nuss and G. M. Air for providing their manuscript prior to publication.

REFERENCES

Alber, T., Dao-pin, S., Wilson, K., Wozniak, J. A., Cook, S. P., & Matthews, B. W. (1987a) Contributions of hydrogen bonds of Thr 157 to the thermodynamic stability of phage T4 lysozyme, *Nature 330*, 41–46.

Alber, T., Dao-pin, S., Nye, J. A., Muchmore, D. C., & Matthews, B. W. (1987b) Temperature-sensitive mutations of bacteriophage T4 lysozyme occur at sites with low mobility and low solvent accessibility in the folded protein, *Biochemistry 26*, 3754–3758.

Amit, A. G., Mariuzza, R. A., Phillips, S. E. V., & Poljak, R. J. (1986) Three-dimensional structure of an antigen–antibody complex at 2.8 Å resolution, *Science 233*, 747–753.

Anderson, D. E., Becktel, W. J., & Dahlquist, F. W. (1990) pH-induced denaturation of proteins: a single salt bridge contributes 3–5 kcal/mol to the free energy of folding of T4 lysozyme, *Biochemistry 29*, 2403–2408.

Arevalo, J. H., Stura, E. A., Taussig, M. J., & Wilson, I. A. (1993) Three-dimensional structure of an anti-steroid Fab′ and progesterone-Fab′ complex, *J. Mol. Biol. 231*, 103–118.

Baker, A. T., Varghese, J. N., Laver, W. G., Air, G. M., & Colman, P. M. (1987) Three-dimensional structure of neuraminidase of subtype N9 from an avian influenza virus, *Proteins 2*, 111–117.

Baker, E. N., & Hubbard, R. E. (1984) Hydrogen bonding in globular proteins, *Prog. Biophys. Mol. Biol. 44*, 97–179.

Bentley, G. A., Boulot, G., Riottot, M. M., & Poljak, R. J. (1990) Three-dimensional structure of an idiotope anti-idiotope complex, *Nature 348*, 254–257.

Bhat, T. N., Bentley, G. A., Fischmann, T. O., Boulot, G., & Poljak, R. J. (1990) Small rearrangements in structures in Fv and Fab fragments of antibody D1.3 on antigen binding, *Nature 347*, 483–485.

Bode, W., & Huber, R. (1991) Ligand binding: proteinase–protein inhibitor interactions, *Curr. Opin. Struct. Biol. 1*, 45–52.

Breyer, R. M., & Sauer, R. T. (1989) Mutational analysis of the fine specificity of binding of monoclonal antibody 51F to λ repressor, *J. Biol. Chem. 264*, 13355–13360.

Bruccoleri, R. E., & Karplus, M. (1987) Prediction of the folding of short polypeptide segments by uniform conformational sampling, *Biopolymers 26*, 137–168.

Chothia, C. (1974) Hydrophobic bonding and accessible surface area in proteins, *Nature 248*, 338–339.

Colman, P. M. (1988) Structure of antibody-antigen complexes: implications for immune recognition, *Adv. Immunol. 43*, 99–132.

Colman, P. M., Laver, W. G., Varghese, J. N., Baker, A. T., Tulloch, P. A., Air, G. M., & Webster, R. G. (1987) Three-dimensional structure of a complex of antibody with influenza virus neuraminidase, *Nature 326*, 358–363.

Colman, P. M., Tulip, W. R., Varghese, J. N., Tulloch, P. A., Baker, A. T., Laver, W. G., Air, G. M., & Webster, R. G. (1989) Three-dimensional structures of influenza virus neuraminidase–antibody complexes, *Philos. Trans. R. Soc. London B323*, 511–518.

Connolly, M. L. (1983) Analytical molecular surface calculation, *J. Appl. Crystallogr. 16*, 548–558.

Cunningham, B. C., & Wells, J. A. (1993) Comparison of a structural and functional epitope, *J. Mol. Biol. 234*, 554–563.

Cunningham, B. C., Henner, D. J., & Wells, J. A. (1990) Engineering human prolactin to bind to the human growth hormone receptor, *Science 247*, 1461–1465.

Dao-pin, S., Sauer, U., Nicholson, H., & Matthews, B. W. (1991) Contributions of engineered surface salt bridges to the stability of T4 lysozyme determined by directed mutagenesis, *Biochemistry 30*, 7142–7153.

Davies, D. R., Padlan, E. A., & Sheriff, S. (1990) Antibody–antigen complexes, *Annu. Rev. Biochem. 59*, 439–473.

Estell, D. A., Graycar, T. P., Miller, J. V., Powers, D. B., Burnier, J. P., Ng, P. G., & Wells, J. (1986) Probing steric and hydrophobic effects on enzyme–substrate interaction by protein engineering, *Science 233*, 659–663.

Fersht, A. R. (1988) Relationship between apparent binding energies measured in site-directed mutagenesis experiments and energetics of binding and catalysis, *Biochemistry 27*, 1577–1580.

Fersht, A. R., Shi, J.-P., Knill-Jones, J., Lowe, D. M., Wilkinson, A. J., BLow, D. M., Brick, P., Carter, P., Waye, M. M. Y., & Winter, G. (1985) Hydrogen bonding and biological specificity analysed by protein engineering, *Nature 314*, 235–238.

Fischmann, T. O., Bentley, G. A., Bhat, T. N., Boulot, G., Mariuzza, R. A., Phillips, S. E. V., Tello, D., & Poljak, R. J. (1991) Crystallographic refinement of the three-dimensional structure of the Fab D1.3–lysozyme complex at 2.5 Å resolution, *J. Biol. Chem. 266*, 1915–1920.

Getzoff, E. D., Tainer, J. A., Lerner, R. A., & Geysen, H. M. (1988) The chemistry and mechanism of antibody binding to protein antigens, *Adv. Immunol. 43*, 1–98.

Gruen, L. C., McInerney, T. L., Webster, R. G., & Jackson, D. C. (1993) Binding affinity of influenza virus N9 neuraminidase with Fab fragments of monoclonal antibodies NC10 and NC41, *J. Protein Chem. 12*, 255–259.

Haneef, I. (1990) Calculation of binding energies using a robust molecular mechanics technique: application to an antibody–antigen complex, *J. Mol. Graphics 8*, 45–51.

Herron, J. N., He, X.-M., Ballard, D. W., Blier, P. R., Pace, P. E., Bothwell, A. L. M., Voss, E. W., & Edmundson, A. B. (1991) An autoantibody to single-stranded DNA; comparison of the three-dimensional structures of the unliganded Fab and a deoxynucleotide–Fab complex, *Proteins 11*, 159–175.

Horton, N., & Lewis, M. (1992) Calculation of the free energy of association for protein complexes, *Protein Sci. 1*, 169–181.

Janin, J., & Chothia, C. (1990) The structure of protein–protein recognition sites, *J. Biol. Chem. 265*, 16027–16030.

Jin, L., Fendly, B. M., & Wells, J. A. (1992) High resolution functional analysis of antibody–antigen interactions, *J. Mol. Biol. 226*, 851–865.

Kabat, E. A., Wu, T. T., Reid-Miller, M., Perry, H. M., & Gottesman, K. S. (1987) *Sequences of proteins of im-*

munological interest, 4th ed., U.S. Public Health Service, National Institutes of Health, Washington, D.C.

Krystek, S., Bruccoleri, R. E., & Novotny, J. (1991) Stabilities of leucine zipper dimers estimated by an empirical free energy method, *Int. J. Pept. Protein Res. 38*, 229–236.

Krystek, S., Stouch, T., & Novotny, J. (1993) Affinity and specificity of serine endopeptidase–protein inhibitor interactions: empirical free energy calculations based on X-ray crystallographic structures, *J. Mol. Biol. 234*, 661–679.

Laskowski, M., Jr., Park, S. J., Tashiro, M., & Wynn, R. (1989) Design of highly specific inhibitors of serine proteases, in *Protein recognition of immobilized ligands: UCLA Symposia on Molecular and Cellular Biology* (Hutchens, T. W., Ed.) Vol. 80, pp 149–160, A. R. Liss, New York.

Lee, B., & Richards, F. M. (1971) The interpretation of protein structures: estimation of static accessibility, *J. Mol. Biol. 55*, 379–400.

Lerner, R. A., Benkovic, S. J., & Schultz, P. G. (1991) At the crossroads of chemistry and immunology: catalytic antibodies, *Science 252*, 659–667.

Lewis, M., & Rees, D. C. (1985) Fractal surfaces of proteins, *Science 230*, 1163–1165.

Lowman, H. B., Cunningham, B. C., & Wells, J. A. (1991) Mutational analysis and protein engineering of receptor-binding determinants in human placental lactogen, *J. Biol. Chem. 266*, 10982–10988.

Murphy, K. P., Xie, D., Garcia, C., Amzel, L. M., & Freire, E. (1993) Structural energetics of peptide recognition: angiotensin II/antibody binding, *Proteins 15*, 113–120.

Nicholls, A., Sharp, K. A., & Honig, B. (1991) Protein folding and association: insights from the interfacial and thermodynamic properties and hydrocarbons, *Proteins 11*, 281–296.

Novotny, J. (1991) Protein antigenicity: a thermodynamic approach, *Mol. Immunol. 28*, 201–207.

Novotny, J., & Sharp, K. (1992) Electrostatic fields in antibodies and antibody/antigen complexes, *Prog. Biophys. Mol. Biol. 58*, 203–224.

Novotny, J., Handschumacher, M., Haber, E., Bruccoleri, R., Carlson, W. B., Fanning, D. W., Smith, J. A., & Rose, G. D. (1986) Antigenic determinants in proteins coincide with surface regions accessible to large probes (antibody domains), *Proc. Natl. Acad. Sci. U.S.A. 83*, 226–230.

Novotny, J., Bruccoleri, R. E., & Saul, F. A. (1989) On the attribution of binding energy in antigen–antibody complexes McPC603, D1.3, and HyHEL-5, *Biochemistry 28*, 4753–4749.

Nuss, J. M., Bossart, P. J., & Air, G. M. (1993) Identification of critical contact residues in the NC41 epitope of a subtype N9 influenza neuraminidase, *Proteins 15*, 121–132.

Padlan, E. A., Silverton, E. W., Sheriff, S., Cohen, G. H., Smith-Gill, S. J., & Davies, D. R. (1989) Structure of an antibody–antigen complex: crystal structure of the HyHEL-10 Fab lysozyme complex, *Proc. Natl. Acad. Sci. U.S.A. 86*, 5938–5942.

Pickett, S. D., & Sternberg, M. J. E. (1993) Empirical scale of side chain conformational entropy ion protein folding, *J. Mol. Biol. 231*, 825–839.

Privalov, P. L., & Makhatadze, G. I. (1993) Contribution of hydration to protein folding thermodynamics II. The entropy and Gibbs energy of hydration (1993) *J. Mol. Biol. 232*, 660–679.

Riechmann, L., Clark, M., Waldmann, H., & Winter, G. (1988) Reshaping human antibodies for therapy, *Nature 332*, 323–327.

Rini, J. M., Schulze-Gahmen, U., & Wilson, I. A. (1992) Structural evidence for induced fit as a mechanism for antibody–antigen recognition, *Science 255*, 959–965.

Sheriff, S., Silverton, E. W., Padlan, E. A., Cohen, G. H., Smith-Gill, S. J., Finzel, B. C., & Davies, D. R. (1987) Three-dimensional structure of an antibody–antigen complex, *Proc. Natl. Acad. Sci. U.S.A. 84*, 8075–8079.

Smith, A. M., & Benjamin, D. C. (1991) The antigenic surface of staphylococcal nuclease II. Analysis of the N-1 epitope by site-directed mutagenesis, *J. Immunol. 146*, 1259–1264.

Smith-Gill, S. J., Wilson, A. J., Potter, M., Prager, E. M., Feldmann, R. J., & Mainhart, C. R. (1982) Mapping the antigenic epitope for a monoclonal antibody against lysozyme, *J. Immunol. 128*, 314–322.

Stanfield, R. L., Fieser, T. M., Lerner, R. A., & Wilson, I. A. (1990) Crystal structures of an antibody to a peptide and its complex with peptide antigen at 2.8 Å, *Science 248*, 712–719.

Sternberg, M. J. E., & Chickos, J. S. (1994) Protein side chain conformational entropy derived from fusion data—comparison with other empirical scales, *Protein Eng. 7*, 149–155.

Tulip, W. R., Varghese, J. N., Baker, A. T., van Donkelaar, A., Laver, W. G., Webster, R. G., & Colman, P. M. (1991) The refined atomic structures of N9 subtype influenza virus neuraminidase and escape mutants, *J. Mol. Biol. 221*, 487–497.

Tulip, W. R., Varghese, J. N., Laver, W. G., Webster, R. G., & Colman, P. M. (1992a) Refined crystal structure of the influenza virus N9 neuraminidase–NC41 Fab complex, *J. Mol. Biol 227*, 122–148.

Tulip, W. R., Varghese, J. N., Webster, R. G., Laver, W. G., & Colman, P. M. (1992b) Crystal structures of two mutant neuraminidase–antibody complexes with amino-acid substitutions in the interface, *J. Mol. Biol. 227*, 149–159.

Turner, G. J., Galacteros, F., Doyle, M. L., Hedlund, B., Pettigrew, D. W., Turner, B. W., Smith, F. R., Moo-Penn, W., Rucknagel, D. L., & Ackers, G. K. (1992) Mutagenic dissection of hemoglobin cooperativity: effects of amino acid alteration on subunit assembly of oxy and deoxy tetramers, *Proteins 14*, 333–350.

Webster, R. G., Air, G. M., Metzger, D. W., Colman, P. M., Varghese, J. N., Baker, A. T., & Laver, W. G. (1987) Antigenic structure and variation in an influenza virus N9 neuraminidase, *J. Virol. 61*, 2910–2916.

Wells, J. A. (1991) Systematic mutational analyses of protein–protein interfaces, *Methods Enzymol. 202*, 390–411.

Williams, D. H., Cox, J. P. L., Doig, A. J., Gardner, M., Nicholls, I. A., Salter, C. J., & Mitchell, R. C. (1991) Toward the semiquantitative estimation of binding constants. Guides for peptide–peptide binding in aqueous solution, *J. Am. Chem. Soc. 113*, 7020–7030.

Wilson, C., Mace, J. E., & Agard, D. A. (1991) Computational method for the design of enzymes with altered substrate specificity, *J. Mol. Biol. 220*, 495–506.

Winter, G., & Milstein, C. (1991) Man-made antibodies, *Nature 349*, 293–299.

Yang, A. S., Sharp, K. A., & Honig, B. (1992) Analysis of the heat capacity dependence of protein folding, *J. Mol. Biol. 227*, 889–900.